Electron transport across fractal-like nanocrystalline clusters in N + ion-beam induced poly(phenylene oxide)

A. Das, S. Dhara, and A. Patnaik

Citation: The Journal of Chemical Physics **114**, 8573 (2001); doi: 10.1063/1.1364704
View online: http://dx.doi.org/10.1063/1.1364704
View Table of Contents: http://scitation.aip.org/content/aip/journal/jcp/114/19?ver=pdfcov
Published by the AIP Publishing

Articles you may be interested in

Molecular self ordering and charge transport in layer by layer deposited poly (3,3-dialkylquarterthiophene) films formed by Langmuir-Schaefer technique
J. Appl. Phys. **116**, 094311 (2014); 10.1063/1.4894515

Morphology and chain aggregation dependence of optical gain in thermally annealed films of the conjugated polymer poly[2-methoxy-5-(2′-ethylhexyloxy)-p-phenylene vinylene]
J. Appl. Phys. **113**, 233509 (2013); 10.1063/1.4811532

Effects of solvents and vacancies on the electrical hysteresis characteristics in regioregular poly(3-hexylthiophene) organic thin-film transistors
Appl. Phys. Lett. **94**, 223302 (2009); 10.1063/1.3148332

Amorphous phase formation, spinodal decomposition, and fractal growth of nanocrystals in an immiscible Hf–Nb system studied by ion beam mixing and atomistic modeling
J. Appl. Phys. **103**, 084910 (2008); 10.1063/1.2912718

Thermally stimulated photoluminescence in poly(2,5-dioctoxy p-phenylene vinylene)
J. Appl. Phys. **91**, 5016 (2002); 10.1063/1.1464235

This article is copyrighted as indicated in the article. Reuse of AIP content is subject to the terms at: http://scitation.aip.org/termsconditions. Downloaded to IP: 130.133.66.132 On: Wed, 26 Nov 2014 13:37:01

Electron transport across fractal-like nanocrystalline clusters in N^+ ion-beam induced poly(phenylene oxide)

A. Das
Department of Chemistry, Indian Institute of Technology Madras, Chennai-600036, India

S. Dhara
Materials Science Division, Indira Gandhi Centre for Atomic Research, Kalpakkam-603102, India

A. Patnaik[a)]
Department of Chemistry, Indian Institute of Technology Madras, Chennai-600036, India

(Received 17 November 2000; accepted 20 February 2001)

Nanocrystalline carbonaceous cluster evolution and electron transport in the N^+ beam induced spin coated poly(2,6-dimethyl-1,4-phenylene oxide) thin films as a function of ion fluence has been investigated. Following Robertson's model and electron diffraction, the narrow optical band gaps were explained in terms of polyaromatic, single crystalline graphitelike clusters. With a threshold fluence of 1×10^{15} ions/cm^2 for cluster growth, the size of the clusters ranged from 2 to 50 nm with the number of aromatic rings varying between 20 and 170 over the entire fluence range upto 8×10^{16} ions/cm^2. A molecular reconstruction/self organization has been envisaged as a possible clue to the above structure evolution upon a critical energy density transferred to the 53 nm implanted layer. Transmission electron microscopy study of fractal scaling in the nanoparticle aggregates revealed a fractal dimension of 1.37 ± 0.02 with the growth process to follow a diffusion limited aggregation model. Electrical conductivity data are explained in terms of a phase transition from an insulating state to a trap controlled hopping conduction of charge carriers between localized states on the backbone cluster with a backbone fractal exponent ~3. © *2001 American Institute of Physics.* [DOI: 10.1063/1.1364704]

INTRODUCTION

Organic molecular thin films have attracted attention in view of their potential applications in electronic devices. Recently, the method of ion-implantation with a precise dopant concentration and accurate depth profiling of the dopant level in the implanted layer has emerged as a promising technique towards insulator–semiconductor transition. The onset of electronic conductivity and optical blackening in the ion-implanted polymers are attributed to the formation of carbonaceous clusters along the latent track of energetic ions upon a threshold energy density deposition. The process of ion track overlapping induces modification in the basic chemical polymer structure.[1] It has been proposed that[2–4] the small spherical carbon-enriched clusters of 10–50 nm diameter at separations ~0.1–20 nm are the carriers of electronic conductivity in the implanted polymers between which the charge carriers tunnel or hop.

Conduction mechanism in semiconductor powders was shown to depend on the degree of sintering[5] implying that at higher interconnection between particles, the schottkey barrier vanishes because of larger area of contact. Thus fractal characterization at a nanoscopic level predicted their macroscopic behavior. There is special interest in fractal concept for polymeric materials; fractal hopping time distributions were studied for thin films of poly methyl methacrylate and polystyrene polymers.[6] However, there is little evidence in literature about the growth of carbonaceous materials in fractal patterns due to beam interaction, though fractal nature was conceptualized to explain the ion-beam induced electrical conductivity.[7]

In our recent report,[8] fractal nature of the nanosized carbonaceous clusters formed in N^+ implanted coated poly(2,6-dimethyl-1,4-phenylene oxide) (PPO) with varying sizes between 2 and 50 nm was discussed. Depending on the predominant energy transfer mode and the energy density transferred, it was proposed that above a critical temperature (corresponding to a dose $\geqslant1\times10^{15}$ ions/cm^2), thermodynamic relaxation creates the graphitic clusters. In this report with a spectroscopic approach to the electronic structure of the implant layer, details of electron transport across the π-bonded graphite clusters, linked together by different sp^3 bonds in a dielectric matrix is discussed. A fractal formalism[9] is adopted to elaborate the mechanism of electron transport.

EXPERIMENT

The crystalline PPO polymer chain is represented below with oxygen bond angle = 110°.

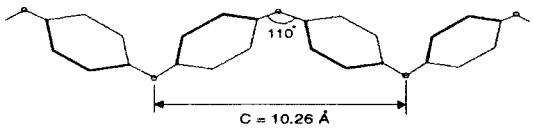

a)Present address: Synchrotron Trieste, S.C.P.A, Trieste, Italy. Electronic mail: archita59@yahoo.com

 © 2001 American Institute of Physics

This article is copyrighted as indicated in the article. Reuse of AIP content is subject to the terms at: http://scitation.aip.org/termsconditions. Downloaded to IP: 130.133.66.132 On: Wed, 26 Nov 2014 13:37:01

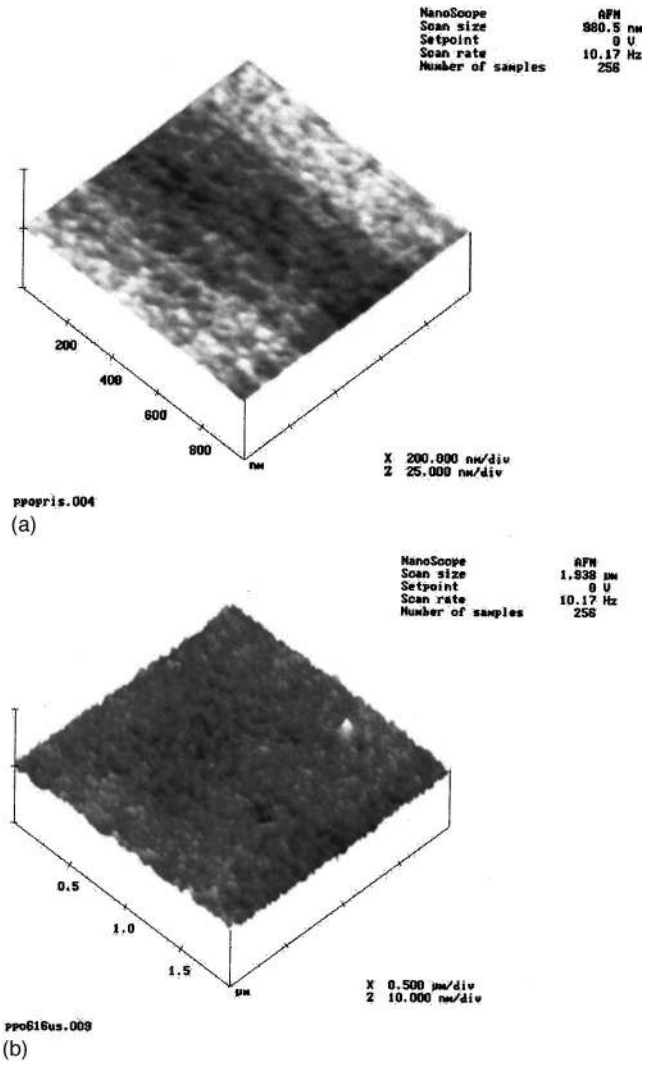

FIG. 1. (a) 3D atomic force microscopy image of the as-deposited PPO film. (b) 3D atomic force microscopy image of the N^+ ion implanted PPO film at a fluence 6×10^{16} ions/cm^2.

Spin coating technique was applied for the preparation of thin films of PPO (Aldrich Co, USA, Mol.wt.40,000) from a $CHCl_3$ solution at room temperature with rotation speeds between 200 and 5000 rpm on quartz, NaCl and Si(100) substrates. Highly homogeneous films with good chemical and topological homogeneity with thickness ~400 nm were made with optimized spin rate and the concentration of the polymer solution. Figure 1(a) shows the 3D (three-dimensional)-atomic force microscopy image of the film deposited on Si(100) at room temperature in a scan scale of 1 μm, confirming the connectivity of the film. The estimated root-mean-square (rms) roughness for this as-deposited film is found to be 16.8 Å with an average roughness of 13.4 Å. Figure 1(b) shows the atomic force microscopy (AFM) image of the maximum dosed implanted sample. In Fig. 2, Raman spectra of the film and the pristine bulk are shown. Raman vibrational modes for PPO were not reported before. In case of aromatic polymers, characteristic vibrational frequencies were assigned in comparision with benzene and its derivatives.[10] Accordingly, 1603, 1438, 1317, and 1231 cm^{-1} features were attributed to —C═C— of the phenyl

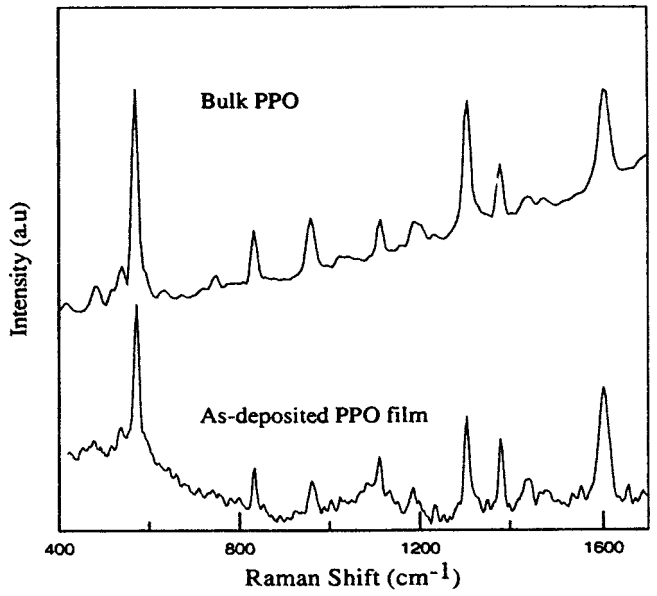

FIG. 2. Raman spectra of the pristine bulk PPO and the as-deposited PPO film.

ring, to the deformation of CH_3 group and to the CH_3–C mode of the substituted methyl group on the benzene ring, respectively. Features at 1204 and 1196 cm^{-1} are assigned to —C–O–C— asymmetric and symmetric stretch modes, respectively. The Raman active band at 1186 cm^{-1} is due to C–H bending and the strong feature at 1112 cm^{-1} may be due to CH_3–C mode for the methyl group present in the ring. 832 cm^{-1} band is due to C–C stretch of the ring and the strong line at 569 cm^{-1} stands for C–C deformation of the ring. These various modes closely resemble the features of bulk PPO and confirm the intactness of the polymeric nature of the film. X-ray diffraction analysis revealed amorphization introduced into the film as a result of stereochemical alteration in the matrix upon solvent interaction.

PPO films were bombarded with 100 keV N^+ ions with a beam current 1 μA on an area of 1 cm^2 under a vacuum of 1×10^{-6} mbar. The implantation dose varied between 1×10^{13} to 1×10^{17} ions/cm^2. The Monte Carlo simulated TRIM code[11] calculations, based on Lindhard–Scharff–Schiott (LSS) theory[12] revealed the projected range of 100 keV N^+ in PPO to be 320 nm with longitudinal and lateral stragglings of 53 and 55 nm, respectively. Accordingly, 400 nm thick films were made for ultraviolet/(UV/VIS), TEM and conductivity measurements. In comparision to the asdeposited film, the dosed implanted sample in Fig. 1(b) shows a certain ordering with formation of columnar features and nano-sized grains with diameter ~50 nm at an improved resolution. The columnar features are attributed to have originated from the erosion of the pristine surface leaving small islands of materials protruding to small heights above the surface. Thus flat grains with well defined size as seen for the pristine material are converted to different shapes after ion-implantation.

Analytical transmission electron microscopy (Philips CM200 along with EDAX detector with super ultra thin window) was performed for studying the morphology and crys-

This article is copyrighted as indicated in the article. Reuse of AIP content is subject to the terms at: http://scitation.aip.org/termsconditions. Downloaded to IP: 130.133.66.132 On: Wed, 26 Nov 2014 13:37:01

tal structure of the pristine and the implanted samples. The crystalline nature of the clusters were probed by microdiffraction method with a probe diameter of 75 nm. Optical spectra were recorded with UV/VIS/NIR Shimadzu PC 3101 spectrometer. Direct current (dc) conductivity measurements were carried out in a temperature range of 80–280 K by van der pauw method under a vacuum of 10^{-3} mbar.

RESULTS AND DISCUSSION

The reorganization of the polymer backbone upon N^+ implantation has induced metamorphic changes in the pristine polymer properties illustrated by the appearance of ~13 orders of conductivity increase associated with a carbon enriched matrix, identified as *a*-C:H (amorphous hydrogenated carbon). The simulation code revealed an inelastic energy transfer of N^+ ion to the matrix to be 28.58 eV/Å at 100 keV energy along with 4.73 eV/Å through elastic nuclear encounters in single ion encounter.

Microstructure of the implanted layer studied by Fourier Transform-Raman (FT) spectroscopy

Local bonding in the implanted layer was inferred from FT-Raman spectra acquired at various doses. The characteristic vibrations of the pristine structure as shown in Fig. 2 were completely lost upon implantation and a broad feature at ~1400–1500 cm^{-1}, beyond a dose 1×10^{15} ions/cm^2 emerged. The deconvolution of the experimental curves for various doses yielded Fig. 3(a). According to the momentum conservation selection rule, a Raman band at 1580 cm^{-1}, known as ''*G*'' band is observed in graphite with large microcrystals.[13,14] An additional peak at 1360 cm^{-1}, known as ''*D*'' line was seen in the Raman spectra of graphite and disordered carbons and was attributed to phonons near the Brillouin zone boundary, active in small crystallites or boundaries of large crystallites. Both bands are found to be present in *a*-C:H whose linewidths are related to the bond angle disorder and to the presence of relative amounts of crystallites in the amorphous matrix. It is reported[15] that both coordinates of carbon, the threefold sp^2 hybridized and fourfold sp^3 hybridized, and the bond angle disorder produce a shift of peaks to lower frequencies. *G* line shift to 1528 cm^{-1} is reported to be associated with a bond angle change from the ideal 120° to the disordered average of 117.7°. The shift in the *G* line in Fig. 3(a) from 1592 to 1528 cm^{-1} is thus attributed to bond angle distortion induced by the implanted ions. In Fig. 3(b), the increase in I_D/I_G ratio is interpreted as growth of the graphitic crystallites in size and in number density which will be confirmed from our TEM results. This enhancement is also reported for ion-induced polystyrene[16] confirming the resulting layer close to the properties of *a*-C:H materials.

The structural transformation induced by ion implantation can not be governed by conventional equilibrium thermodynamics since the duration that bombarded ions come to stop in the surface layer and get dissipated is $\sim10^{-10}$ s. It was suggested[17] that structural similarity leading to structural transformation plays a more important role than thermodynamic factors during beam induced transformation. From this stand point, the conversion from aromatic rings into hexagonal graphitic cells is favorable and is due to their high degree of structural similarity such as bond lengths and planar hexagonal geometry. Upon ion irradiation, the partially displaced ions with free radicals have a high probability of recombination with vacancies forming fused rings, dimers, trimers, etc. Thus, the originally isolated aromatic rings condense into clusters of aromatic rings leading to a graphitelike structure.

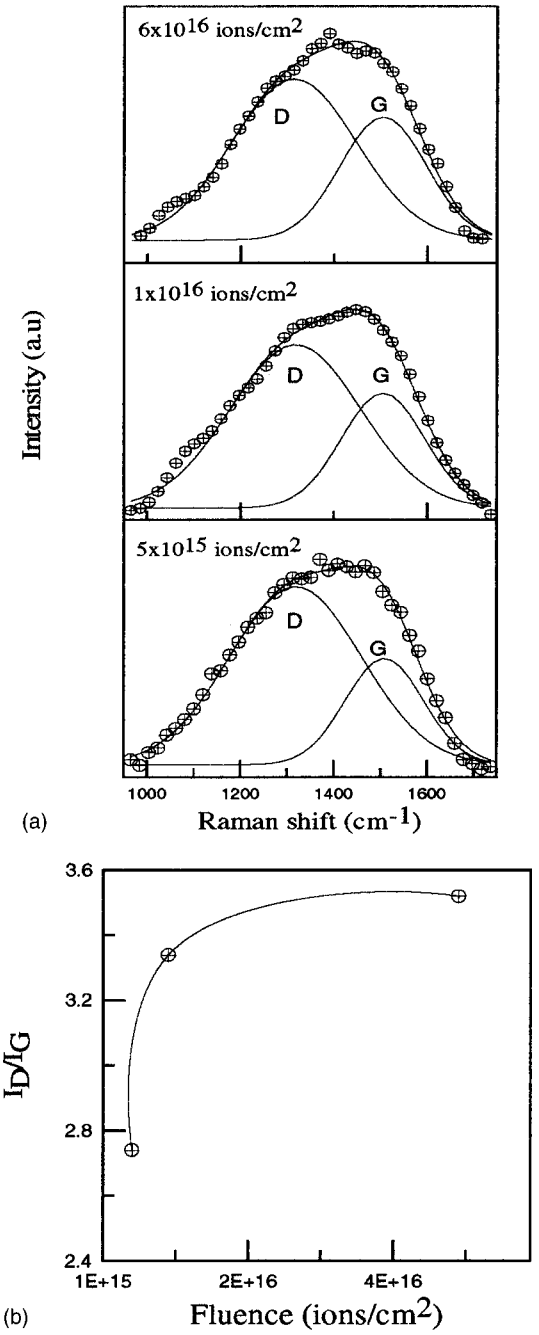

FIG. 3. (a) Deconvoluted Raman spectra of 100 keVN^+ implanted PPO films at various fluences. (b) Ratios of the integrated intensities of the *D* and *G* lines in the deconvoluted Raman spectra as a function of fluence.

Imaging of the N^+-beam implanted PPO films by transmission electron microscopy

The as-deposited PPO film, coated with ~5 nm Au for charge dispersion, showed a honey-comb structure in the

This article is copyrighted as indicated in the article. Reuse of AIP content is subject to the terms at: http://scitation.aip.org/termsconditions. Downloaded to IP: 130.133.66.132 On: Wed, 26 Nov 2014 13:37:01

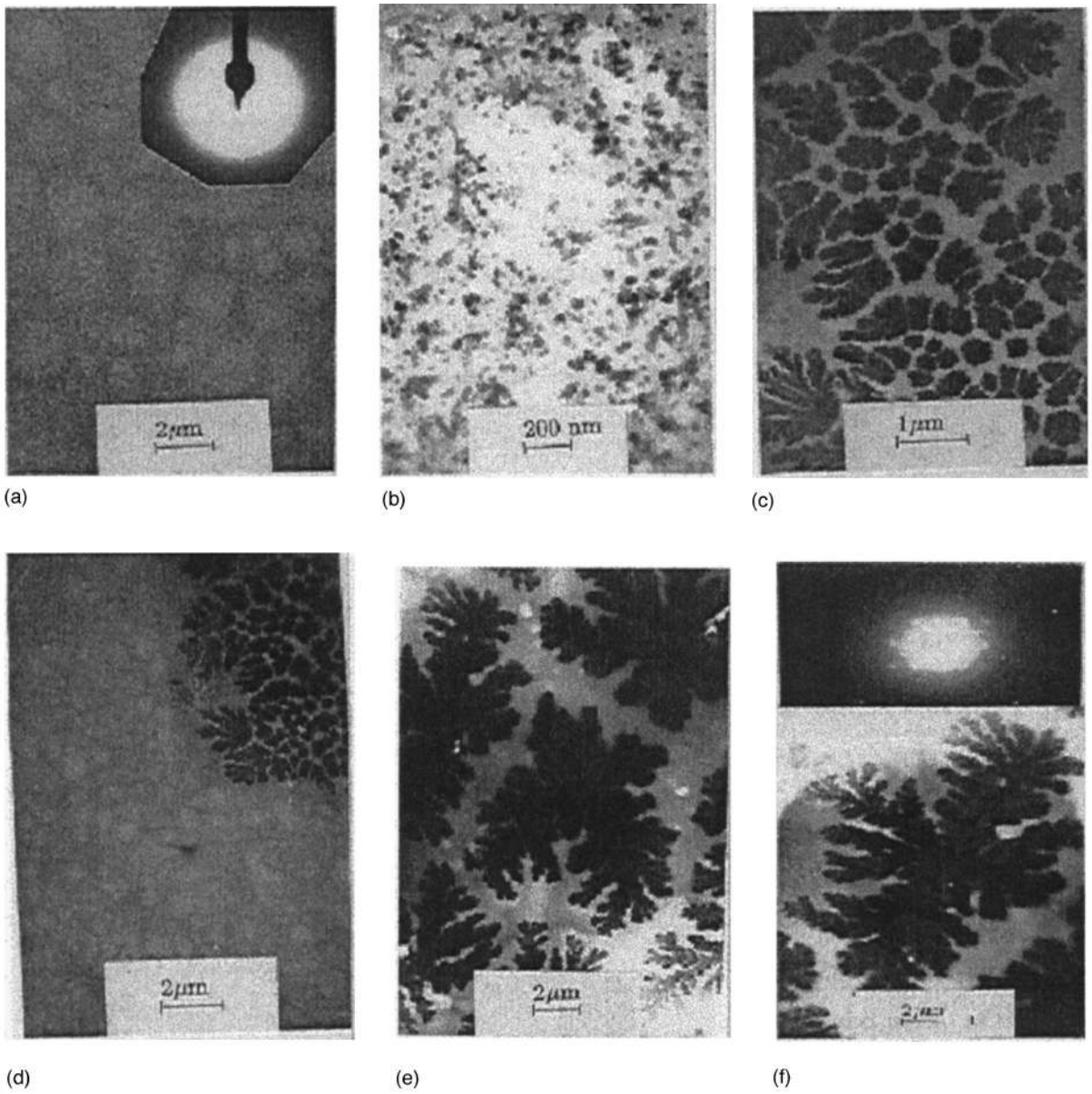

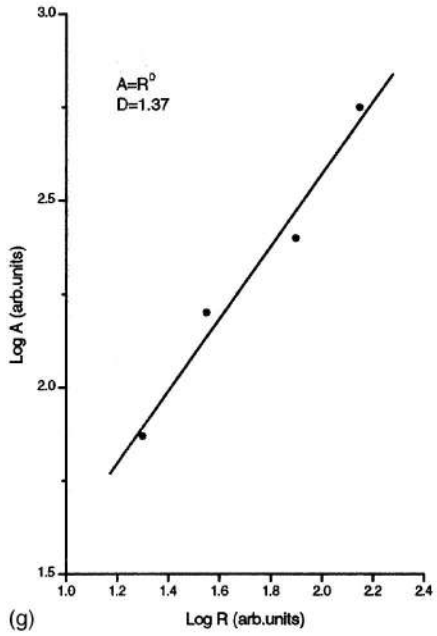

FIG. 4. (a) TEM image of the PPO as-deposited film. Microdiffraction pattern of the amorphous phase is shown in the inset. (b) Ramified growth of carbonaceous clusters of PPO film implanted at a fluence of 1×10^{15} ions/cm^2. (c) TEM image of the N^+ implanted PPO film indicating growth of carbonaceous clusters in fractal pattern at a fluence of 1×10^{16} ions/cm^2. (d) Micrograph of the PPO film implanted at 1×10^{16} ions/cm^2 showing the existence of featureless matrix and clusters. (e) TEM image of the PPO film implanted at a fluence of 6×10^{16} ions/cm^2 showing growth of larger fractal patterns containing carbonaceous clusters. (f) Amplified micrograph of the PPO film implanted at a fluence of 6×10^{16} ions/cm^2. The outset shows micro-diffraction of the clusters. (g) Derivation of fractal dimension for the N^+ implanted PPO film from the log–log plot for A vs R.

This article is copyrighted as indicated in the article. Reuse of AIP content is subject to the terms at: http://scitation.aip.org/termsconditions. Downloaded to IP: 130.133.66.132 On: Wed, 26 Nov 2014 13:37:01

TABLE I. Parameters obtained from SAED (selected area diffraction) patterns of implanted PPO films and their comparision with JCPDS data for graphite (JCPDS card no. 22-1069).

Sample	*d*-spacings (Å)	*hkl*	*d*-spacings (Å)	*hkl*	Angle	Zone axis
Graphite (JCPDS)	3.71	(104)	3.22	(201)	50.09°	⟨070⟩
1×10^{16} ions/cm^2	3.48 ± 0.17	(104)	2.97 ± 0.16	(201)	51.5°	⟨070⟩
6×10^{16} ions/cm^2	3.43 ± 0.19	(104)	2.88 ± 0.18	(201)	51.8°	⟨070⟩

bright field image of the TEM [see Fig. 4(a)]. Micro diffraction pattern of the film at different locations showed broad and diffuse ring patterns [inset of Fig. 4(a)], characteristic of the amorphous phase. Presence of amorphous phase in the pristine spin cast film, as indicated by x-ray diffraction (XRD) studies, has also been reported earlier.[18] The structural transformation to 100% amorphous nature from a 34% crystalline polymer powder in $CHCl_3$ solution is attributed to the possible conformational change on the $CHCl_3$ solvated monomer skeleton.

Microstructural features of the implanted layer at a dose of 1×10^{15} ions/cm^2 in Fig. 4(b) showed the presence of two distinct phases. The growth of ramified fractal pattern was surrounded by a featureless structure as shown in the bright field image. A large number of clusters are distributed in the matrix and overlap of these clusters have given rise to possible fractal pattern. The sizes of these clusters as measured from the images vary between 2 and 15 nm.

With an increase in dose to 1×10^{16} ions/cm^2, larger inelastic energy deposition resulted in increasing the size and number density of the above mentioned clusters in the film as shown in Fig. 4(c). The fractal pattern at this dose is clear in the bright field image of TEM. In Fig. 4(d), coexistence of the carbonaceous matrix with the newly grown fractal pattern is seen. With further increase in the ion dose to 5×10^{16} ions/cm^2, the size of the fractal pattern increased from 5 to 6 μm and is shown in Fig. 4(e). In the dark field image of a selected zone, the cluster sizes varied from ~30 nm to a maximum of ~50 nm in an assembly of islands of clusters. Average size and the number density of these clusters were found to increase with dose, indicating enhanced amounts of carbon condensation. The amplified micrograph along with the microdiffraction pattern of these clusters are shown in Fig. 4(f). The latter evidences the signature of resulting single crystalline phase. Structural analysis of these crystalline particles resembled the graphitic carbon structure. The interplanar spacing (d) of the (hkl) plane for the hexagonal system was calculated according to Andrews *et al.*[19] as

$$1/d^2=\frac{4}{3a^2}(h^2+hk+k^2)+\frac{1}{c^2}(l^2), \tag{1}$$

with a and c as lattice parameters. The angle ϕ between $(h_1k_1l_1)$ and $(h_2k_2l_2)$ is given by

$$\cos\phi=\frac{h_1h_2+k_1k_2+\frac{1}{2}(h_1k_2+k_1h_2)+\frac{3}{4}\frac{a^2}{c^2}l_1l_2}{\sqrt{\left(h_1^2+k_1^2+h_1k_1+\frac{3a^2}{4c^2}l_1^2\right)\left(h_2^2+k_2^2+h_2k_2+\frac{3a^2}{4c^2}l_2^2\right)}}. \tag{2}$$

The zone axis was found to be along ⟨070⟩ direction. Thus, a single crystalline, graphitelike carbonaceous cluster growth was confirmed as an effect of N^+ implantation above a critical dose of 1×10^{15} ions/cm^2. The calculated d-spacings from the single crystalline spot patterns for implantation doses 1×10^{16} and 6×10^{16} ions/cm^2 were compared with graphite and are presented in Table I.

Fractal growth in the N^+ implanted film

By processing the TEM images, we tried to understand the geometry and structural property of the surface by determining the fractal dimension by manual box counting. The variation of area coverage (A) as a function of radius of gyration (R) is shown in Fig. 4(g) for the 6×10^{16} ions/cm^2 implanted PPO film. From the log–log plot, $A=R^D$ is satisfied with dimension $D=1.37\pm0.02$. The value is comparable to fractal dimension of 1.30 ± 0.075 reported for two-dimensional growth of clusters through diffusion limited aggregation (DLA) on fibers.[20] In the growth process of fractals in PPO, as observed over a wide N^+ ion fluence, the precipitation of carbonaceous phase at a threshold dose $\sim1\times10^{15}$ ions/cm^2 marks the beginning and further agglomerates to the fractal form. In the framework of DLA model, fractal structures are formed as a result of irreversible aggregation of small particlelike clusters with their diffusion to surface as the rate limiting step during aggregation or non-equilibrium growth process. Primary particles diffuse randomly up, to be captured by a growing agglomerate–fiber and remain anchored in the place of collision. The fragmented polymer molecules and the cross-linked materials upon irradiation are reported[21] to possess fibrous structure which helps in aggregation of nanocrystalline graphitic particles to aggregate in fractal form over a large dose range and upon a large magnitude of energy deposition.

Optical spectroscopy evidencing cluster formation in the N^+ ion implanted PPO layer

Optical absorption in the UV/V is region as a powerful tool was adopted to understand the electronic properties and

This article is copyrighted as indicated in the article. Reuse of AIP content is subject to the terms at: http://scitation.aip.org/termsconditions. Downloaded to IP: 130.133.66.132 On: Wed, 26 Nov 2014 13:37:01

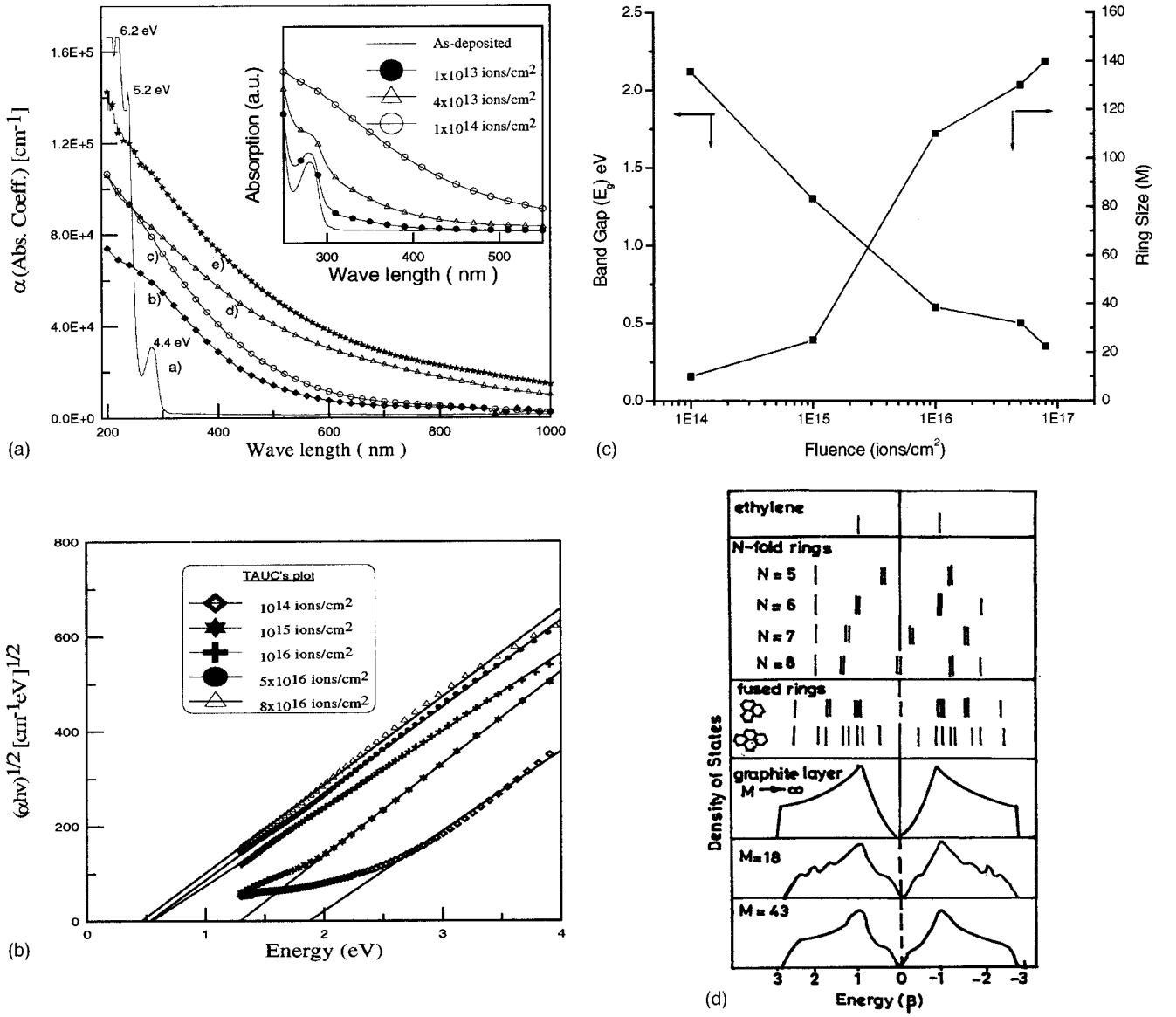

FIG. 5. (a) Absorption spectra of the (a) as-deposited and N^+ implanted PPO films with fluence (b) 10^{14}, (c) 10^{15}, (d) 10^{16}, and (e) 6×10^{16} ions/cm^2. Inset shows the disappearance of the 4.4 eV feature. (b) Determination of optical band gap(E_g) as a function of fluence in the N^+ implanted PPO film. (c) Variation of optical band gap and ring size with fluence in the N^+ implanted PPO film. (d) Electronic states and spectra of carbon bonding configurations according to Ref. 13.

the optical band gap of the formed a-C:H in the implanted layer. The atomic and electronic structures are closely related in a-C:H[22] and of particular interest is the presence of π states and the effect of their disordering. Since these states are weakly bound, they lie close to the Fermi level E_F than the σ states, opening the highest occupied molecular orbital–lowest unoccupied molecular orbital (HOMO–LUMO) gap. The filled π states form the valence band and the empty π^* states, the conduction band; thus, controlling the size of the band gap.

The absorption spectra of the pristine and the N^+ implanted samples at various doses are shown in Fig. 5(a). Three prominent features accompany the pristine film as reported by La Femina *et al.*[23] These transitions, dipole forbidden in benzene, are dipole allowed in the reduced symmetry of PPO. The peak at 4.4 eV derives from benzene $^1A_{1g}\rightarrow{}^1B_{2u}$ transition, the peak at 5.2 eV from the $^1A_{1g}\rightarrow{}^1B_{1u}$ transition and the large feature at 6.2 eV consists of benzene dipole allowed $^1A_{1g}\rightarrow{}^1E_{1u}$ transition. Absorption falls rapidly in an exponential manner over the entire dose range due to transitions between localized states and band states (will be narrated in the next section) and the exponential dependence arises from the exponential density of state (DOS) distribution in the band structure of a-C:H.[24] The inset in Fig. 5(a) shows slow destruction of $^1A_{1g}\rightarrow{}^1B_{2u}$ transition at 4.4 eV with increasing dose. At a minimum dose $\sim1\times10^{14}$ ions/cm^2, all characteristic features disappear and the absorption coefficient increases with increasing dose and with shifting of the absorption edge to higher wavelengths. For aliphatic and linear polymers such as poly methyl methacrylate, the shift of the absorption edge to visible region was attributed to an enhancement in the conjugation length,[25] whereas, for aromatic polymers such as polystyrene,[26,27] condensation of aromatic rings into compact carbonaceous clusters was

This article is copyrighted as indicated in the article. Reuse of AIP content is subject to the terms at: http://scitation.aip.org/termsconditions. Downloaded to IP: 130.133.66.132 On: Wed, 26 Nov 2014 13:37:01

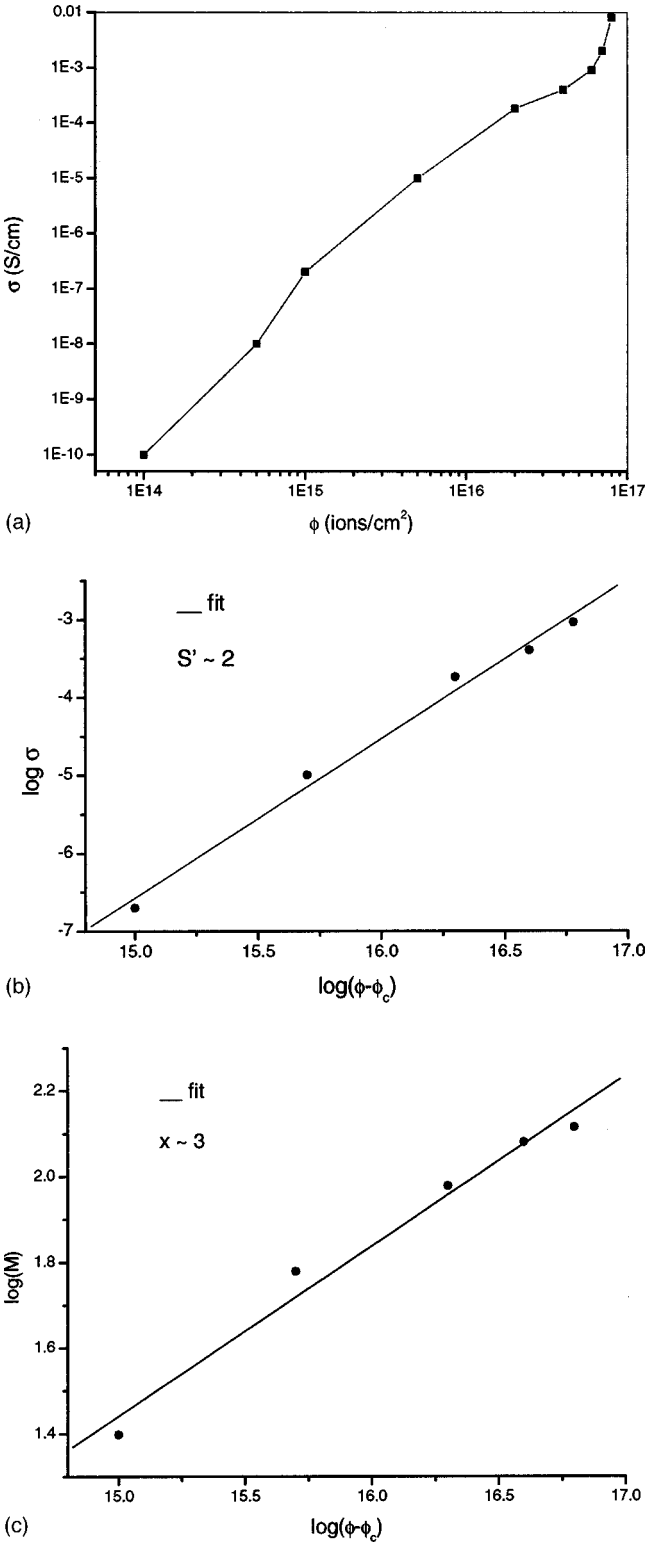

FIG. 6. (a) Variation of room temperature conductivity with N^+ ion fluence in the PPO films. (b) Theoretical fit for the fluence dependence of conductivity for PPO films at 100 keV. (c) Theoretical fit for the fluence dependent cluster size distribution for PPO films at 100 keV.

stated as a possible explanation. The increased absorption can arise from an enhancement in the carrier concentration or because of the formation of metallic clusters at doses $>10^{15}$ ions/cm^2.

Tauc's formula was used to determine the optical band gaps (E_g), shown in Fig. 5(b) as a function of dose. An obvious and progressive decrease in the E_g values from 2.12 to 0.45 eV over a dose range 1×10^{14} to 1×10^{17} ions/cm^2 is observed in Fig. 5(c) with a saturation at higher doses. The effective optical gaps of the implanted films were used to characterize their short and medium range order. This issue has been reported in details by Robertson and O'Reilly[28] who showed that the optical gap can be correlated to the number, type and structural arrangement of carbon bonds. In the framework of Huckel approximation, they mapped the electronic structure of a-C:Hs with sp^2 and sp^3 sites into a network of π-states with minimum coupling between σ and π states and further into a series of independent clusters, while considering the adjacent interaction of the planar sp^2 sites. Consequently, a correlation between the optical band gap E_g and M, the number of six membered rings constituting the sp^2 bonded fragments was brought as

$$E_g = 2\beta/M^{1/2}, \tag{3}$$

with β as the nearest-neighbor interaction between the π orbitals of the six membered rings and was taken as a constant$=-2.9$ eV. Figure 5(c) depicts a progressive increase in the average size of the clusters as a function of dose. The cluster formation begins at a threshold dose $\sim1\times10^{15}$ ions/cm^2 with $M=10$ and increases further to as high as 140 at 6×10^{16} ions/cm^2.

The graphitelike nature of the clusters were confirmed[28] by calculating the π binding energies and the electronic spectra of a wide range of possible structures along with graphite. In Fig. 5(d), the DOS of finite layers of fused benzene rings with number of rings $M=18$ resembles that of graphite layer with $M=\infty$ and with $M=43$, the spectrum is smooth. Thus π bonding strongly favored aromatic rings over olefinic chains with a preference for clustering of the former to graphitic sheets. Hence, fused sixfold ring conformation was preferred for the N^+ beam induced formation of clusters in the implanted PPO film.

N^+ ion dose dependent conductivity in the implanted layer

In the previous sections, we reported the self organization of the implanted polymer layer into two distinct phases at and above a critical dose. The presence of band gap required the aromatic clusters/sp^2 domains not to percolate through the essentially planar layer of 53 nm, but remain as islands. The σ states with the two center bonds formed the backbone of the random network. We measured the dc conductivity of this layer as a function of dose and the profile is shown in Fig. 6. An increasing trend in conductivity with dose is observed with the maximum reaching $\sim10^{-2}$ S/cm at a dose 8×10^{16} ions/cm^2.

The dc conductivity in PPO upon 200 keVBr^+, As^+, Kr^+, and N^+ implantation was explained[7] in terms of inter group transition probabilities within the damage blob with high local concentration of free radicals and the mechanism was associated with trap controlled hopping of the charge carriers. The mechanism also explained lagging of the percolation threshold dose for conductivity compared to the sharp onset of the free radical concentration, supported from

This article is copyrighted as indicated in the article. Reuse of AIP content is subject to the terms at: http://scitation.aip.org/termsconditions. Downloaded to IP: 130.133.66.132 On: Wed, 26 Nov 2014 13:37:01

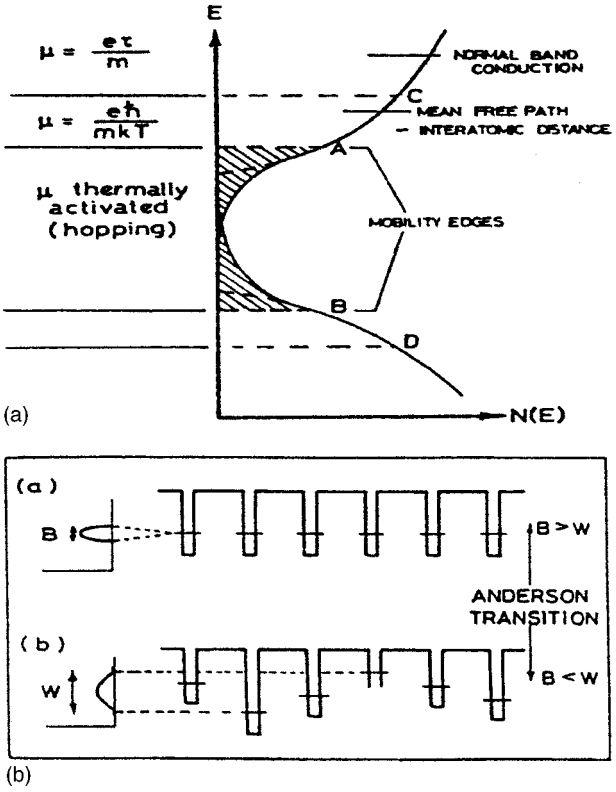

FIG. 7. (a) Schematic representation of the DOS in amorphous semiconductors showing the localized electronic states according to Ref. 29. (b) Potential wells representing localized states; disorder induced localization takes place when the disorder width ''*w*'' exceeds the band width ''*B*,'' according to Ref. 29.

the unpaired spin measurement. Wasserman[7] argued that at low dose range, the rate of radical creation is in dynamical equilibrium with the radical-vacancy recombination through the percolative delocalization of free radicals within the blob. In the intermediate dose range, the sharp transition from insulating to a trap controlled hopping mechanism was supported by the current transient measurements. Complying with the above, in our experiments, although the characteristic UV-VIS absorptions were completely lost at a dose 1×10^{14} ions/cm^2, the onset of sp^2 bonded cluster formation began at 1×10^{15} ions/cm^2 along with the associated conductivity, signifying insulator–semiconductor transition. Assuming the critical dose ϕ_c to be 1×10^{14} ions/cm^2, the fractal exponent S', for conductivity in the experimental fluence range was calculated as

$$\sigma\sim(\phi-\phi_c)^{-S'}, \tag{4}$$

$$\text{with}\quad S'=x\upsilon\tilde{s}=x\upsilon(d_f-d_w), \tag{5}$$

where ''x'' represents the critical exponent reflecting the relation between the cluster size distribution function and the implantation dose via

$$p-p_c\sim(\phi-gf_c)^x \tag{6}$$

with ''p'' as the probability of site occupation by a free radical and p_c, the critical occupation probability. The total cluster mass ''N_F'' was further correlated to $(p-p_c)$ as,

$$N_F\sim(p-p_c)^{-\upsilon d_l} \tag{7}$$

with the chemical or spreading dimension of the damage region, assumed to be 2 in our case since the conductive layer is essentially planar (53 nm), υ is taken as 1/2 classically. N_F can thus be approximated as

$$N_F\sim(\phi-\phi_c)^x. \tag{8}$$

The fit to the experimental data in Fig. 6(b) resulted S' to be ~2. With the cluster sizes obtained from FT-Raman and UV/VIS measurements, we have estimated the critical exponent x to be 2.5 from a plot of $\log M$ (ring size) vs $\log(\phi-\phi_c)$, as shown in Fig. 6(c). d_w, as the fractal dimension of the random walk of a charge carrier within the blob/cluster was calculated to be 1.37 ± 0.02 for a dose 6×10^{16} ions/cm^2 [Fig. 4(g)]. Thus, the back bone fractal exponent d_f was estimated to be ~3 according to Eq. (5).

TABLE II. Parameters derived from Mott's equations for 3D VRH mechanism in the N^+ ion implanted PPO film.

Fluence (ions/cm^2)	8×10^{16}	7×10^{16}	6×10^{16}
T_0 (K)	2.77×10^6	7.57×10^5	1.0×10^4
σ_0 (S/cm)	4.5×10^3	99.5	25.0
$N(E_F)$ (eV^{-1} cm^{-3})	8.13×10^{24}	4.75×10^{18}	8.6×10^{16}
α (cm^{-1})	4.75×10^8	5.56×10^6	1.6×10^5
R_0 (cm) at 100 K	1.0×10^{-8}	1.16×10^{-6}	7.4×10^{-6}
αR	14.75	6.22	1.18
W (eV)	0.031	0.036	0.007

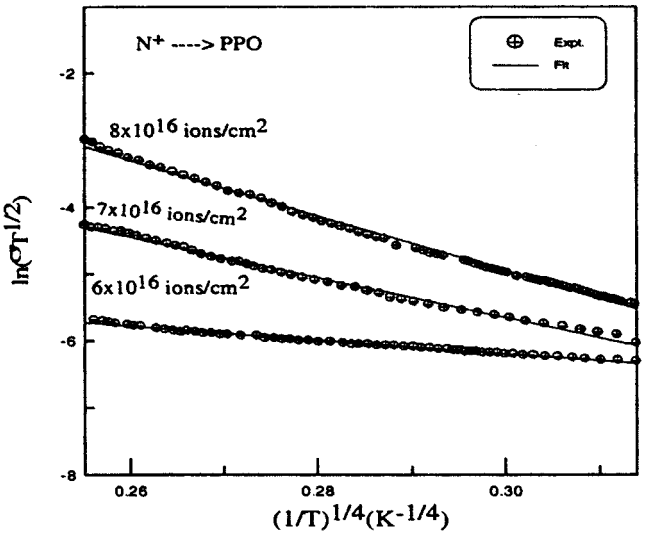

FIG. 8. Least-square fitting of $\ln\sigma T^{-1/2}$ against $T^{-1/4}$ on the basis of 3D VRH process in the N^+ implanted PPO film.

Temperature dependence of electron transport in the N^+ ion implanted PPO layer

The implanted layer with a major amorphous phase as evidenced from the TEM images is envisaged as an amorphous semiconductor. Here, the concept of a forbidden gap with an energy equal to that for breaking covalent bonds between atoms has been accepted.[29] In these materials, the electronic states at the band edges are perturbed on going to the amorphous phase and the density of states is finite in the gap.[30] Figure 7(a) shows a schematic tailing of the states into the gap to a degree in which the bonding valence states and

This article is copyrighted as indicated in the article. Reuse of AIP content is subject to the terms at: http://scitation.aip.org/termsconditions. Downloaded to IP: 130.133.66.132 On: Wed, 26 Nov 2014 13:37:01

the antibonding conduction states overlap near the center of the gap. Electronic states in these tails arise from structural defects and large variations in density and composition throughout the material, similar to the effect from an energetic ion–solid interaction. The levels are distributed over a sufficiently wide energy range V_0, to satisfy the criterion of localization[31] according to

$$V_0 > 10zI\exp(\alpha R), \tag{9}$$

where, z is the coordination number, I, the overlapping integral, R, the mean separation between the centres and α is a measure of the extent of wave functions on isolated centers.

The localized states extend at band extremities upto well defined energies A and B [Fig. 7(a)] with DOS equal to ~20% of that associated with the band. Because the states between A and B are localized, conduction occurs in this energy range only by thermally activated hopping. The mobility associated with this process is small and is given by,

$$\mu = \frac{\lfloor e\upsilon_{\mathrm{ph}} R^2 \exp(-2\alpha R)\exp(-w/kT)\rfloor}{kT}. \tag{10}$$

υ_{ph} is the phonon frequency and w is a measure of the average activation energy required for hopping between localized (quantized) states as represented in Fig. 7(b). The potential wells representing the atomic sites vary with respect to the well depth as compared to a crystalline matrix. The band width B here is much less than the random potential W. In Fig. 7(a), near A and B, w is expected to be small and the tunneling factor $e^{-2\alpha R}$ approaches 1, leading to a maximum mobility of typically ~0.1 $\mathrm{cm^2/V.s}$.[31]

According to Mott's VRH formalism, there is no free motion of charge carriers when they are localized. Hence a predominant conduction proceeds via phonon-assisted hopping of charge carriers between the localized states, A and B at sufficiently low temperatures. The temperature dependent electrical conduction narrated by VRH takes the general form

$$\sigma(T) = \sigma_n(T)\exp\left[-\left(\frac{T_n}{T}\right)^{1/n+1}\right], \tag{11}$$

where σ_n and T_n are characteristic parameters, determined experimentally. The σ_n parameter is a weak function of temperature and thus the conduction process is governed by the exponential term. For VRH conduction, n stands for dimensionality ($n=1,2,3$) and σ_n is proportional to $T^{-2/n+1}$. The temperature dependent conductivity in the temperature range 80–280 K and for doses of 6×10^{16} to 8×10^{16} $\mathrm{ions/cm^2}$, as observed by the present authors, seems to follow a dominant 3D VRH mechanism as evident from Fig. 8. It is worth mentioning here that over a low-temperature range of 80–280 K, the samples associated with a dose $<6\times10^{16}$ $\mathrm{ions/cm^2}$ imparted a very high resistance resulting in poor ohmic contact. Thus, a 3D VRH hopping conduction governed by interaction of charge carriers with the phonons of the fractal network of the conductive clusters was concluded and the associated parameters listed in Table II were calculated as

$$\sigma_0 = 3e^2\upsilon_{\mathrm{ph}}\left[\frac{N(E_F)}{8\pi\alpha k}\right]^{1/2}, \tag{12}$$

$$T_0 = \frac{\lambda\alpha^3}{kN(E_F)}, \tag{13}$$

$$R = \left[\frac{9}{8\pi k\alpha TN(E_F)}\right]^{1/4}, \tag{14}$$

$$w = \frac{3}{4\pi R^3/N(E_F)}. \tag{15}$$

$N(E_F)$ is the density of states near the Fermi level, λ is a dimensionless constant, υ_{ph} is the frequency factor ($\sim 3\times10^{12}\,\mathrm{H_z}$) and R is the hopping distance. It is seen that T_0 as a measure of disorder, complies with the reported value of 10^5–10^7 K.[32] αR, representing the degree of localization of charge carriers in the trap states decreases from 14.75 to 1.18 with fluence, implying a consistency with the VRH requirement of $\alpha R \gg 1$. The $N(E_F)$ values varying from 10^{24} to 10^{16} $\mathrm{eV.cm^{-3}}$ over the dose range are also consistent with the reported value of $\sim10^{18}$ $\mathrm{eV.cm^{-3}}$ in a-C:H with α as 12 A°. The determination of backbone fractal exponent as three possibly serves as a definitive proof for the dimensionality of the medium where the charge transport occurs.

CONCLUSION

The N^+ ion–beam induced evolution of a ~50 nm PPO polymer layer was investigated with respect to its chemical and electronic structures along with its fractal geometry. The implanted layer resembled the a-C:H structure with a network consisting of independent clusters of sp^2 bonded carbon atoms and an sp^3 carbon configuration with H bonded to it. The microcrystalline clusters were investigated to be fused hexagonal and polynuclear aromatic rings in a graphitelike phase, with cluster sizes varying between 2 and 50 nm, whose size and number density depended on the ion fluence. The fluence dependent conductivity was found to be associated with a fractal exponent 2 over the fluence range along with a backbone fractal exponent of 3. Electron transport from temperature dependent conductivity measurements in the temperature range 80–280 K was explained in terms of trap controlled hopping of charge carriers between localized states in a defect band in the mobility gap.

[1] Y. Q. Wang and R. E. Giedd, Nucl. Instrum. Methods Phys. Res. B **79**, 659 (1993).
[2] T. Venkatesan, S. R. Forrest, M. L. Kaplan, C. A. Murray, P. H. Schmidt, and B. J. Wilkens, J. Appl. Phys. **56**, 2778 (1983).
[3] O. Yu. Posudievsky, Radiat. Eff. Defects Solids **137**, 119 (1995).
[4] D. Fink, K. Ibel, P. Goppelt, J. P. Biersack, L. Wang, and M. Behar, Nucl. Instrum. Methods Phys. Res. B **46**, 342 (1990).
[5] J. C. Sanchez-Lopez and A. Fernandez, Acta Mater. **48**, 3761 (2000).
[6] R. Kopelman, L. A. Harmon, E. I. Newhouse, S. J. Parus, and J. Prasad, ''*MRS Symposium on Fractal Aspects of Materials*'' (Boston, 1985) (unpublished).
[7] B. Wasserman, Phys. Rev. B **34**, 1926 (1986).
[8] A. Das, S. Dhara, and A. Patnaik, Phys. Rev. B **59**, 11069 (1999).
[9] H. E. Stanley, J. Stat. Phys. **36**, 843 (1984).
[10] B. H. Stuart, Spectrochim. Acta, Part A **53**, 107 (1997).
[11] J. P. Biersack and L. G. Haggmark, Nucl. Instrum. Methods **174**, 257 (1980).
[12] J. L. Lindhard, M. Scharff, and H. E. Shiott, Mat. Fys. Medd. K. Dan. Vidensk. Selsk. **33**, 14 (1963).
[13] J. Robertson, Adv. Phys. **35**, 317 (1986).

This article is copyrighted as indicated in the article. Reuse of AIP content is subject to the terms at: http://scitation.aip.org/termsconditions. Downloaded to IP: 130.133.66.132 On: Wed, 26 Nov 2014 13:37:01

[14] E. H. Lee, D. M. Hembree, Jr., G. R. Rao, and L. K. Mansur, Phys. Rev. B **48**, 15540 (1993).
[15] D. Beeman, J. Silverman, R. Lynds, and M. R. Anderson, Phys. Rev. B **30**, 870 (1984).
[16] G. Foti and R. Reitano, Nucl. Instrum. Methods Phys. Res. B **46**, 306 (1990).
[17] B. X. Liu, X. Zhou, and H. D. Li, Phys. Status Solidi A **113**, 11 (1989).
[18] A. Das, G. Ghosh, S. Dhara, and A. Patnaik, Mater. Lett. **38**, 82 (1999).
[19] K. W. Andrews, D. J. Dyson, and S. R. Keown, *Interpretation of electron diffraction patterns* (Adams Hilger Ltd., London, 1971), p. 94.
[20] P. Mikin, Phys. Rev. A **27**, 2616 (1983).
[21] G. R. Rao, Z. L. Wang, and E. H. Lee, J. Mater. Res. **8**, 927 (1993).
[22] J. Robertson, Prog. Solid State Chem. **21**, 199 (1991).
[23] J. P. LaFemina, G. Arjavalingam, and G. Hougham, J. Chem. Phys. **90**, 5154 (1989).
[24] G. D. Cody, T. Tiedje, B. Abeles, B. Brooks, and Y. Goldstein, Phys. Rev. Lett. **47**, 1480 (1981).
[25] J. P. Davenas, T. G. Boiteux, M. Fallavier, and X. L. Lu, Nucl. Instrum. Methods Phys. Res. B **46**, 317 (1990).
[26] R. M. Papaleo, M. A. Araujo, and R. P. Livi, Nucl. Instrum. Methods Phys. Res. B **65**, 442 (1992).
[27] X. L. Xu, D. Xu, H. L. Xu, R. Wang, S. C. Zou, G. D. Du, and G. Q. Xia, J. Vac. Sci. Technol. A **12**, 3200 (1994).
[28] J. Robertson and E. P. O'Reilly, Phys. Rev. B **35**, 2946 (1987).
[29] E. A. Davis and R. F. Shaw, J. Non-Cryst. Solids **2**, 406 (1970).
[30] N. F. Mott, Adv. Phys. **16**, 49 (1967).
[31] N. F. Mott, Philos. Mag. **19**, 835 (1969).
[32] R. L. Casalini, M. Goldenberg, C. Pearson, B. K. Tanner, and M. C. Petty, J. Phys. D: Appl. Phys. **31**, 1504 (1998).

This article is copyrighted as indicated in the article. Reuse of AIP content is subject to the terms at: http://scitation.aip.org/termsconditions. Downloaded to IP: 130.133.66.132 On: Wed, 26 Nov 2014 13:37:01